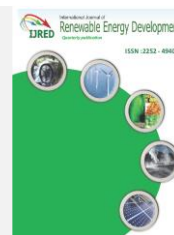




Contents list available at IJRED website





**International Journal of Renewable Energy Development**

Journal homepage: <https://ijred.undip.ac.id>



Research Article

## A four-line active shunt filter to enhance the power quality in a microgrid

Abdelkader Mostefa<sup>1,2\*</sup> , Karim Belalia<sup>1,2</sup> , Tayeb Lantri<sup>1</sup> , Houari Merabet Boulouiha<sup>2</sup> ,  
Ahmed Allali<sup>3</sup> 

<sup>1</sup>Department of Electrical Engineering and Automation, University of Relizane, Relizane, Algeria

<sup>2</sup>Laboratoire de Simulation, Commande, Analyse et Maintenance des Réseaux Electriques(LSCAMRE), National Polytechnic School of Oran-Maurice Audin, Oran, Algeria

<sup>3</sup>Laboratoire de Développement Durable de l'Énergie Électrique(LDDEE), University of Science and Technology Mohamed Boudiaf, Oran, Algeria

**Abstract.** In recent years, power quality has become a major concern for electric network managers. Active filtering control schemes ensure improved power quality of the electric network and are able to maintain a desired voltage level at the point of connection, regardless of the current absorbed by nonlinear loads. Harmonics can cause vibrations, equipment distortion, losses and sweating in transformers. The main objective of this work is to enhance the quality of energy in a microgrid consisting of 100 kW photovoltaic (PV) system and a 50 kW battery storage connected to nonlinear and unbalanced loads. This paper proposes a the four-arm parallel active filter with a on Proportional-Integral (PI) controller to mitigate the harmonic problems in a microgrid. In addition, an algorithm has been designed to eliminate the neutral current. The identification function is one of the most particular approach for extracting harmonics, it involves providing a current reference imposed by the active filter in order to carry out the filtering operation. Both the performance and the quality of the current harmonic compensation's depend strongly on the strategy adopted for the generating the current reference. In this work, the instantaneous power strategy p-q is chosen outstanding the simplicity and effectiveness in implementation. The proposed control strategy has been tested under simulations and the results have shown good tracking of the references and a significant reduction in the Total Harmonic Distorsion (THD) level under highly unbalanced conditions of the nonlinear loads. The current THD is reduced from 43.64 before filtering to 3.74% after the application of the four-arm filter, following the recommendations of IEEE-519 standard (THD less than 5%).

**Keywords:** Harmonic pollution, non-linear load, active parallel filter, neutrality fault, the pq method, quadruple-wire inverter.



© The author(s). Published by CBIORE. This is an open access article under the CC BY-SA license (<http://creativecommons.org/licenses/by-sa/4.0/>).

Received: 15<sup>th</sup> Nov 2022; Revised: 5<sup>th</sup> March 2023; Accepted: 25<sup>th</sup> March 2023; Available online: 3<sup>rd</sup> April 2023

### 1. Introduction

The terminology 'Total Harmonic Distortion' or 'THD' denotes the relative contribution of harmonics to the distortion of an ideal voltage or current waveform. Harmonics can cause a buzz, vibrations, losses, overheating in transformers, and even equipment malfunction. Every power quality problem has a different reason. Some of them are derived from the shared infrastructure. A network failure can cause, for example, a dip that harms some energy consumers connected to the network. The increase in the level of the defect consequently leads to a significant number of affected customers. A problem raised on the site of a customer produces a transient, which can subsequently affect other customers located in the same neighborhood. In addition, problems, such as harmonics, originating within the customer's facility, propagate through the network, and affect other customers. Hence, a combination of good design practices and proven mitigation equipment can solve harmonic problems.

A tool providing an instantaneous analysis of the reactive and active power is required to filter harmonics. Earlier theories

developed in the 1940s served as the foundation for the concepts of apparent, reactive, and active powers among these is the p-q theory or the instantaneous active and reactive power theory (Akagi *et al.* 2017). The p-q theory can also provide compensation for harmonic currents into the electrical grid and simplifies the calculations for active and reactive powers. The p-q theory has been widely used in the literature (Dobrucky *et al.* 2022; Huaman *et al.* 2022 ; Boukadoum *et al.* 2022 ; Rath *et al.* 2022 ; Chennai *et al.* 2022 ; Benedicte *et al.* 2022 ; El Ghaly *et al.* 2022 ; Tsvetanov *et al.* 2022).

Shunt active filters have been extensively used for the attenuation of harmonics. A comparison of simulation and realization results has been studied in (Rohouma *et al.* 2020; Raman *et al.* 2022; Albasri *et al.* 2022). The software used in the practical portion is based on the dSPACEScalexio simulation and is run on a 7.5 kVA test bench. At the Point of Common Coupling (PCC), the current's THD is reduced from 26.88% to 2.99%. As a result of realization, the current's THD is reduced from 26.99 to 3.43%. Active filters are increasingly finding applications in PV systems. Similarly, a series of recent studies including (Goud *et al.* 2021; Devassy *et al.* 2017; Rasul *et al.* 2017;

\* Corresponding author  
Email: [mostefaz006@yahoo.fr](mailto:mostefaz006@yahoo.fr) (A. Mostefa)

Bezerra et al. 2017; Saleh et al. 2021; Azzam-Jai et al. 2019) have investigated the connection between an active shunt filter and a PV farm. The former has shown effectiveness against harmonics against nonlinear loads. Kamala et al. (2018) conducted a study to improve the quality and dependability of the power supply in petrochemical industries using Active Power Filters (APF). However, the cases of unbalanced loads were not considered in all these contributions cited above.

This article focuses on the impact of the shunt active filter with four legs connected to a microgrid which consist of a 100 kW PV farm and an energy storage system based on Lithium-ion batteries. Acharya et al. (2022) proposed an algorithm called nm-Predator Prey Fire-Fly (nm-PPFO) for the reduction of THD. Conventional methods such as Gravitational Search Algorithm (GSA), Particle Swarm Optimization (PSO), and Accelerated PSO have also been applied. The simulation study has been performed under MATLAB/Simulink environment and the results obtained demonstrate the robustness of the proposed method an its effectiveness in reducing harmonics as compared to other techniques. A control scheme was proposed in (Maciel et al. 2018) to mitigate harmonic problems in four-wire three-phase systems based on a two capacitors to a common neutral topology. The neutral point between these two capacitors can be used to eliminate harmonics in the neutral. An active power filter based on a three-level neutral-point clamped (NPC) type T converter with LCL input filter is presented in (Bula et al. 2021). The main objective of this work is to analyze the control of reactive power flow independently and reduce the THD level. The work has been validated experimentally. However, these methods are complicated and/or do not handle the current in the neutral.

In this paper, a simple algorithm is proposed to eliminate the neutral current in a microgrid in a more effective way. The remaining of the paper is organized as follows: Section 2 presents the microgrid system considered in this study. Section 3 presents the control methods of the various system components. Section 4 presents the results of the simulation using MATLAB/Simulink to demonstrate the impact of the filter on the improvement of the energy quality of the microgrid connected with an unbalanced nonlinear load. Section 5 summarises the conclusion of the paper.

## 2. Description and Modeling of the Studied Microgrid System

The microgrid system shown in Figure 1 consists of a PV system with a nominal power 100 kW at 1000W/m<sup>2</sup>, a battery energy storage system with 50 kW nominal power, nonlinear single-phase loads, and an active four-wire shunt filter.

A voltage source inverter with four-leg is used to compensate for the harmonic currents generated by the three arms. The elimination of the current in the neutral is achieved using the fourth leg. The reverse current produced by the inverter is introduced into the system to compensate for the harmonic currents; these currents are obtained using the p-q theory. To achieve neutral current compensation, two main topologies are used: (i) inverters to generate voltages; (ii) Inverters with two midpoint capacitors and a four-arm inverter (used as an active filter) (Barva et al. 2018; Kumar et al. 2022; Collins et al. 2022; Zhang et al. 2022; Challa et al. 2022). Mainly, the four-wire shunt active filters, with three phases, have three branches with two switches controlled by the PWM technique and the fourth leg is on standby and has two switches controlled by the PWM technique. The four-wire converter compensates for the neutral current using an additional bridge, as shown in Figure 1. When the four-leg topology is used in a shunt active filter, it always gives better results because the four-arm inverter drives all three-phase currents and the neutral. On the other hand, the three-arm inverter with midpoint capacitors directly drives only three currents. The fourth one is the result of the sum of the currents on the DC side.

The PV array is modelled using the one-diode equivalent circuit and is described by the following equation (Mankour et al. 2017; Pradhan et al. 2017 ; Rao et al. 2017; Hilali et al. 2022; Asgharian et al. 2019; Diab et al. 2020):

$$I_{pv} = I_{ph} - I_s \left[ e^{\left( \frac{V_{pv} + I_{pv} R_s}{mKT} \right)} - 1 \right] \frac{V_{pv} + I_{pv} R_s}{R_{sh}} \quad (1)$$

Where  $I_{ph}$  represents the photo-current generated by the PV cell (A),  $I_s$  is the diode saturation current or dark current (A),  $V_{pv}$  denotes the voltage applied across the diode (V),  $R_s$  is serial resistance of the PV cell ( $\Omega$ ),  $R_{sh}$  is the parallel or shunt resistance ( $\Omega$ ),  $m$  is the ideality coefficient of the PV cell,  $K$  denotes the Boltzmann constant ( $1,38 \times 10^{-23}$  J/K), and  $T$  is the absolute temperature expressed in Kelvin (K).

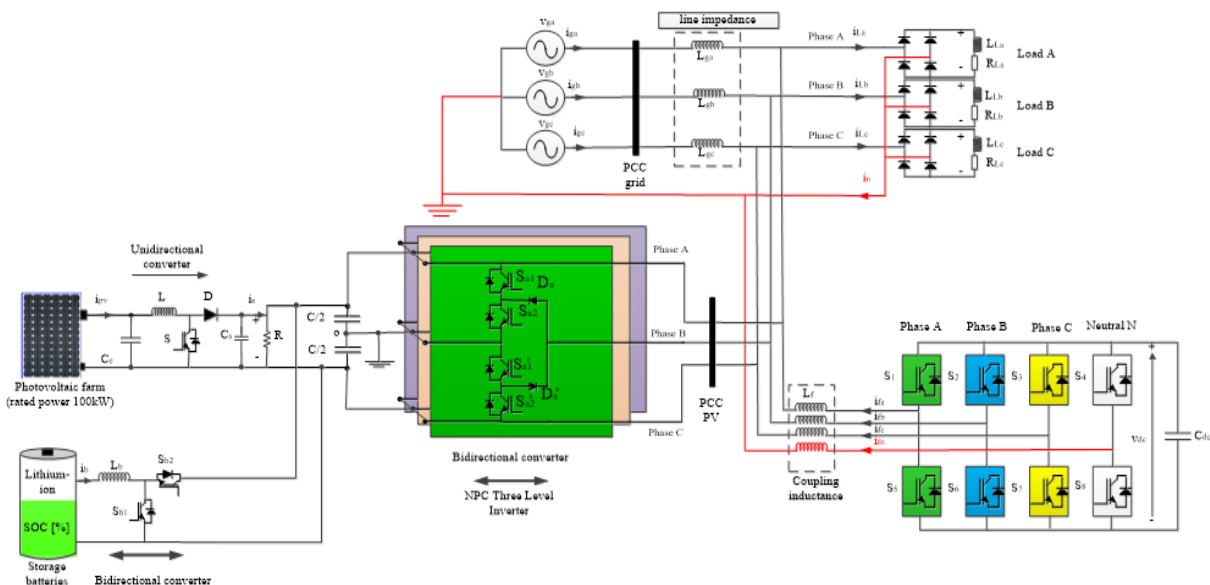


Fig. 1. Micro-grid connected to a non-linear load.

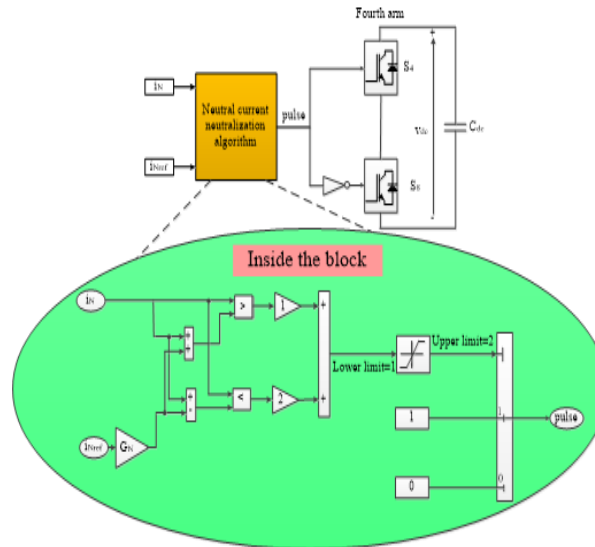


Fig. 2. Control flow chart of the neutralization of the current in the neutral line.

### 3. Proposed Control Scheme

#### 3.1 Control of the four-legs filter

The balanced, symmetrical, non-linear, three-phase loads connected to the neutral produce harmonic currents of order three and multiples of three in this conductor. The effective value of the neutral current may be higher than the phase current (a phase's current value may be up to  $\sqrt{3}$  times). The simplest way to prevent overloading the neutral conductor is to select a neutral conductor with a cross section that is twice that of the phase conductor. The cost and lack of equipment protection are the disadvantages of this strategy. To eliminate the current in the neutral, as illustrated in Figure 2, the integration a fourth leg is proposed.

The instantaneous active and reactive power p-q theory allows the identification of the references currents. The DC component of the instantaneous active and reactive powers is eliminated. Given the three load currents and the voltages of a three-phase network (connected to a polluting load), denoted as  $i_{La}, i_{Lb}, i_{Lc}$  et  $v_{ga}, v_{gb}, v_{gc}$  respectively. The Concordia algebraic transformation of voltage components is:

$$\begin{bmatrix} v_{go} \\ v_{g\alpha} \\ v_{g\beta} \end{bmatrix} = \sqrt{\frac{2}{3}} \begin{bmatrix} \frac{1}{\sqrt{2}} & \frac{1}{\sqrt{2}} & \frac{1}{\sqrt{2}} \\ 1 & -\frac{1}{2} & -\frac{1}{2} \\ 0 & \frac{\sqrt{3}}{2} & -\frac{\sqrt{3}}{2} \end{bmatrix} \begin{bmatrix} v_{ga} \\ v_{gb} \\ v_{gc} \end{bmatrix} \quad (2)$$

The current components are:

$$\begin{bmatrix} I_{Lo} \\ I_{L\alpha} \\ I_{L\beta} \end{bmatrix} = \sqrt{\frac{2}{3}} \begin{bmatrix} \frac{1}{\sqrt{2}} & \frac{1}{\sqrt{2}} & \frac{1}{\sqrt{2}} \\ 1 & -\frac{1}{2} & -\frac{1}{2} \\ 0 & \frac{\sqrt{3}}{2} & -\frac{\sqrt{3}}{2} \end{bmatrix} \begin{bmatrix} I_{La} \\ I_{Lb} \\ I_{Lc} \end{bmatrix} \quad (3)$$

The following relation defines the instantaneous active and reactive powers, denoted p and q, respectively (De Araujo Ribeiro et al. 2014; Hoon et al. 2016; Tounsi et al. 2021):

$$\begin{bmatrix} p \\ q \end{bmatrix} = \begin{bmatrix} v_{g\alpha} & v_{g\beta} \\ -v_{g\beta} & v_{g\alpha} \end{bmatrix} \begin{bmatrix} i_{L\alpha} \\ i_{L\beta} \end{bmatrix} \quad (4)$$

Generally, the powers p and q each comprise a continuous part and a relative part, allowing to write the following expression:

$$\begin{cases} p = \bar{p} + \tilde{p} \\ q = \bar{q} + \tilde{q} \end{cases} \quad (5)$$

$\bar{p}$ : A continuous power related to the active fundamental component of current and voltage.

$\bar{q}$ : A continuous power related to the fundamental component of tension and reactive current.

$\tilde{p}$  and  $\tilde{q}$ : Alternating powers related to the total of the unsettling current and voltage components.

In our article, these components are denoted by:  $p_{ref} = \bar{p} + p_c$  and  $q_{ref} = \bar{q}$ , where  $p_c$  is the DC bus voltage regulator's output. Using the relation (4);

$$\begin{bmatrix} \tilde{i}_{L\alpha} \\ \tilde{i}_{L\beta} \end{bmatrix} = \begin{bmatrix} v_{g\alpha} & -v_{g\beta} \\ v_{g\beta} & v_{g\alpha} \end{bmatrix}^{-1} \begin{bmatrix} \tilde{p} \\ \tilde{q} \end{bmatrix} \quad (6)$$

Define the determinant of the matrix as  $\Delta = v_{g\alpha}^2 + v_{g\beta}^2$  (Khalid et al. 2020; Hasan et al. 2017 ; Kumar et al. 2020) then:

$$\begin{cases} \tilde{i}_{L\alpha} = \frac{v_{g\alpha}}{\Delta} \tilde{p} - \frac{v_{g\beta}}{\Delta} \tilde{q} \\ \tilde{i}_{L\beta} = \frac{v_{g\beta}}{\Delta} \tilde{p} + \frac{v_{g\alpha}}{\Delta} \tilde{q} \end{cases} \quad (7)$$

Based on these equations, a notification that from the expression of  $i_\alpha$  and  $i_\beta$  the homopolar power is absent. The current homopolar is defined as:

$$\begin{cases} i_{f\alpha ref} = \tilde{i}_{L\alpha} \\ i_{f\beta ref} = \tilde{i}_{L\beta} \\ i_{fo ref} = i_o \end{cases} \quad (8)$$

Where:  $i_o$  is a current homopolar component.

The neutral current should be noted  $i_n$  and the homopolar current  $i_o$  are linked by the following relationship:

$$\begin{cases} i_n = i_{La} + i_{Lb} + i_{Lc} \\ i_o = \frac{1}{\sqrt{3}}(i_{La} + i_{Lb} + i_{Lc}) = \frac{1}{\sqrt{3}}i_n \end{cases} \quad (9)$$

Finally, it is very easy to derive the currents of reference by the Concordia inverse transformation:

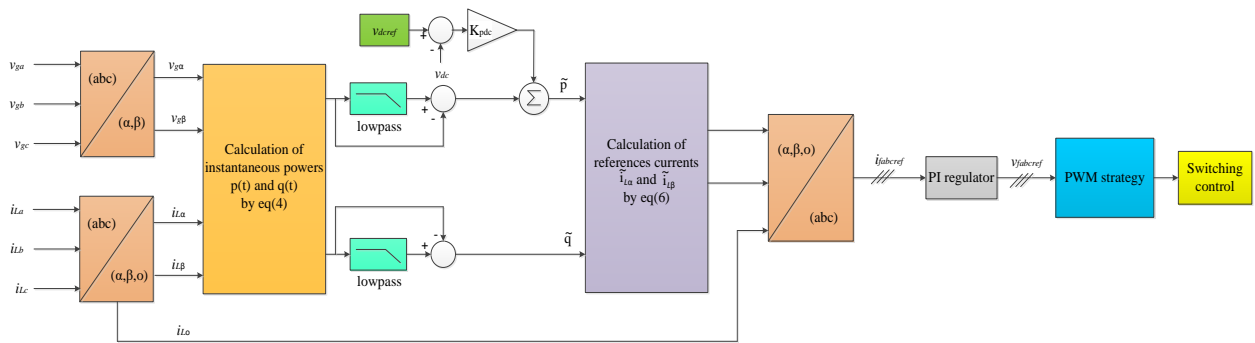


Fig. 3. Utilizing the instantaneous power technique for identification.

Table 1  
Transfer functions for the strategy of PI controllers.

Regulator of	Reference R	Disturbance D	Transfer function G(s)	Output Y
Current of the filter	d-axis $i_{fdref}$ q-axis $i_{fqref}$	0	$\frac{1}{L_f s}$	$i_{fd}$ $i_{fq}$
Current of the batteries	$i_{bref}$	0	$\frac{1}{L_b s}$	$i_b$
DC voltage of the filter	$v_{dc ref}$	0	$\frac{1}{C s}$	$v_{dc}$

$$\begin{bmatrix} i_{faref} \\ i_{fbref} \\ i_{fc ref} \end{bmatrix} = \sqrt{\frac{2}{3}} \begin{bmatrix} 1 & 0 & \frac{1}{\sqrt{2}} \\ -\frac{1}{2} & \frac{\sqrt{3}}{2} & \frac{1}{\sqrt{2}} \\ -\frac{1}{2} & -\frac{\sqrt{3}}{2} & \frac{1}{\sqrt{2}} \end{bmatrix} \begin{bmatrix} i_{fdref} \\ i_{fqref} \\ i_{fref} \end{bmatrix} \quad (10)$$

Fig. 3 shows the detailed diagram of the shunt active filter control (Belalia et al. 2021).

The main concept is to add in the direct loop control, upstream a proportional regulator ( $K_{pdc}$ ) is used to keep the DC voltage bus and requires the current to follow its references generated by the strategy PQ. Current regulation consists of enslaving the currents from the network (indirect control of the  $i_{gabc}$  network). The instantaneous power method is only applicable if the network voltage is perfectly sinusoidal and balanced. The first step is to bring the voltage of the  $v_{gabc}$  network and the currents of the  $i_{Labc}$  load into the Concordia frame. This transformation makes it possible to switch from a three-phase system to a two-phase system, which simplifies the mathematical expressions.

The design of all the PI regulators is based on this scheme: All regulators are synthesized from Fig.4. The control loops are chosen rigorously. For example, outer loops are laid faster than inner loops to ensure overall control system stability. This constraint determines the choice of the gains of the PI regulators in order to ensure good tracking of the references.

In this case, the synthesis applied in the paper for determining the gains of the PI regulators uses pole placement and is presented in Table 1.

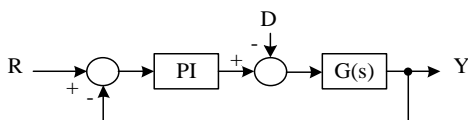


Fig. 4 Scheme of the PI regulators.

### 3.2 MPPT strategy

The method of incremental inductance is used in this work. It consists of finding the slope of the power and voltage curve at the Maximum Power Point (MPP). This is done by calculating the derivative of the power of the PV panel in relation to the voltage and set it to zero. The slope is positive to the left of the MPP point and negative to the right as shown in Table 2 (Patel et al. 2020; Nayak et al. 2017; Başoğlu et al. 2022; de Jesus et al. 2019).

### 3.3 Direct Power Control (DPC)

Based on the objectives highlighted above, the renewable energy system has been dimensioned and controlled to adapt the battery charging and discharging control algorithms according to climatic conditions and load demands to ensure system reliability.

Figure 5 shows the power and control circuit for power management between the hybrid PV/battery storage system and the loads, with four different operating modes based on the PV generation, which depends on the irradiation and the temperature. The DC output of the PV generator side converter (rectifier to PWM) is connected to the DC bus. This is directly connected to the battery bank. The energy exchanges of the system are therefore carried out on the DC bus between PV-battery-load-grid.

The block  $C_b(s)$  represents the function of the PI regulator and is expressed as:

$$C_b(s) = kp_b + \frac{k_{ib}}{s} \quad (11)$$

A bidirectional buck-boost converter connects the battery to the DC bus. An algorithm is responsible for controlling the battery charge and discharge, which gives the command for the selection of either buck-mode or boost-mode. The bounds of the algorithm are set in between 40-80% to increase battery life duration as shown in Figure 6 (Zhang et al. 2021; Olabi et al. 2022; Amini et al. 2019; Wu et al. 2022; Okay et al. 2022).

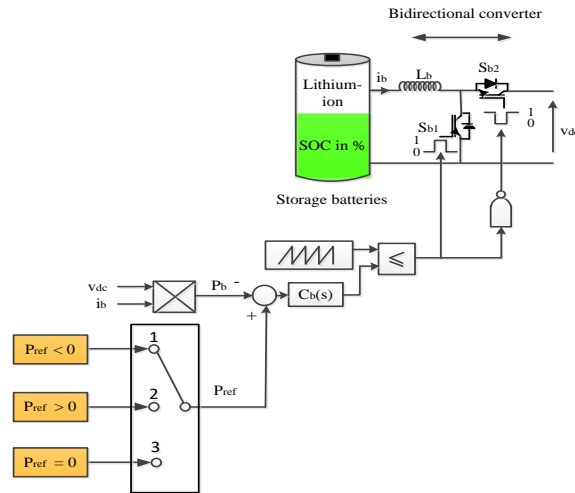


Fig.5. Flowchart describing the different operating modes of the PV system with battery storage.

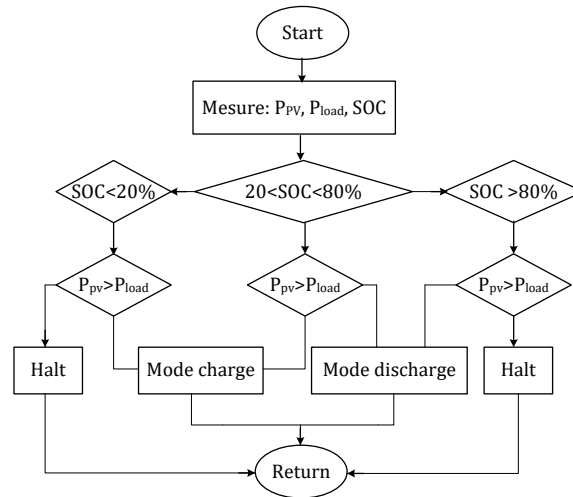


Fig.6. Block diagram of different operating modes of the photovoltaic system with battery storage.

Table 2

Steps of the MPPT inductance increment method.

The solar panel's power is provided by:
$P=V.I$
The partial derivative $\frac{dP}{dV}$ is given by :
$\frac{dP}{dV} = V \frac{dI}{dV} + I$
$\frac{dP}{dV} = V \frac{dI}{dV} + I \cong V \frac{\Delta I}{\Delta V} + I$
$\frac{\Delta I}{\Delta V} = -\frac{I}{V}$ in MPP
$\frac{\Delta I}{\Delta V} > -\frac{I}{V}$ at the left of MPP
$\frac{\Delta I}{\Delta V} < -\frac{I}{V}$ at the right of the MPP

#### 4. Results and discussion

Two scenarios were carried out to test the four-leg active filter and the efficiency of the PV+battery microgrid (Table 3 shows the parameter values of the simulated model.). The method of identifying instantaneous powers to detect the reference harmonic currents is used in the simulation. Besides, the cut-off frequency of the second order low pass extraction filter is set to 50Hz and all switching (for the DC-DC or DC-AC converters) are controlled by PWM strategy.

##### 4.1 Study of filter efficiency

The overall system includes a PV generator with the boost converter controlled by MPPT control and the storage system controlled by a bidirectional buck/boost converter. The non-linear unbalanced load has been connected in the AC side (between the PV-Batteries system and the distribution network). The following single-phase loads are considered: (i) for phase A:  $R_a = 4 \Omega$ ,  $L_a = 0.07 H$ ; (ii) for phase B:  $R_b = 6 \Omega$  and  $L_b = 0.04 H$ ; (iii) finally phase C:  $R_c = 8 \Omega$  and  $L_c = 0.06 H$ . The

**Table 3**  
Parameters used in simulation.

System	Designation	Values
Power supply	The effective voltage	$V_s = 220 \sqrt{2} \text{ V}$
	The frequency	$f = 50 \text{ HZ}$
	Internal resistance	$R_s = 0.1 \text{ m}\Omega$
	Internal inductance	$L_s = 1 \mu\text{H}$
Parallel power active filter	Storage capacitor de	$C_{dc} = 2.5 \text{ mF}$
	Output filter	$L_f = 1 \text{ mH}$
	Reference voltage	$V_{dc\_ref} = 900 \text{ V}$
DPF Control Parameters	DC bus voltage regulator	$k_c = 100$
	Reference current PI regulator	$k_p = 300$
		$k_i = 35$
		$T_e = 4 \mu\text{s}$
Simulation Conditions	Sampling time	variable step
	Type of step	ode15s (stiff / NDF) (NDF)
	Resolution method	2KHz
	Switching frequency (PWM)	5000
Converter DC/DC	Inductance $L_b$ (H)	0.003
	Switching frequency (Hz)	5000
Regulator $C_b$ (s)	Proportional gain $K_{pb}$	0.005
	Integral gain $K_{ib}$	0.001
Lithium-ion Battery	Nominal voltage (V)	48
	Capacitor (Ah)	6.5

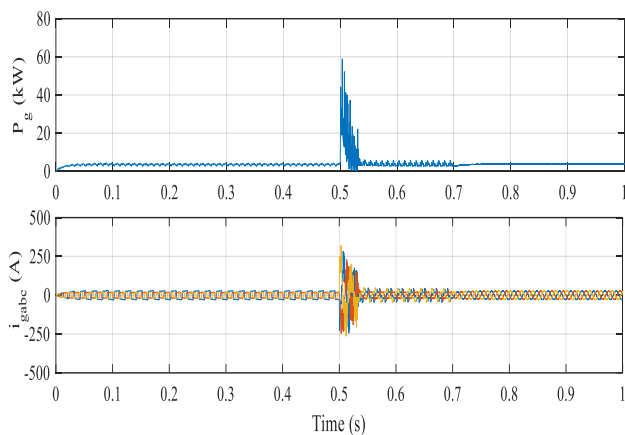


**Fig.7** Responses of the power and the three-phase current of the grid.

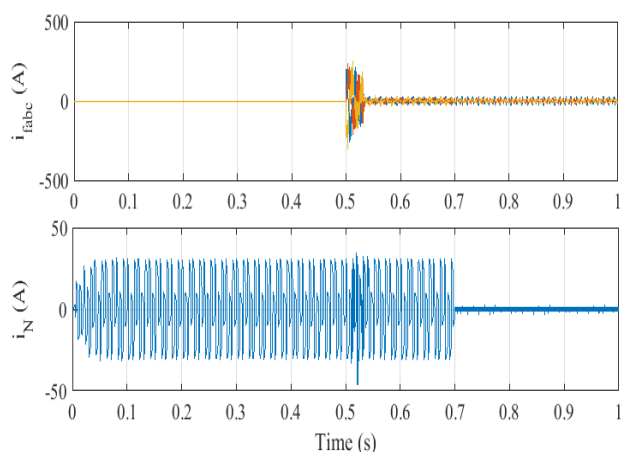


**Fig.8** Three-phase current supplied from the filter and the neutral current.

active power and the three-phase currents of the grid are shown in Fig. 7.

The unbalanced current in the load generates a current in the neutral where the sum of the three-phase currents is not zero. Before using the neutral current neutralization procedure,

the current imbalance is clearly visible. Due to the existing imbalance between non-linear loads; the network current is not sinusoidal even if an active filter is used at time  $t=0.5\text{s}$ . As shown in Figure 8, it can be noticed that the current in the neutral is not zero because of the unbalance of the nonlinear loads in the time range  $[0, 0.7\text{s}]$ .

After using the neutralization algorithm, the neutral current becomes zero and thus the network current becomes sinusoidal at time  $t = 0.7 \text{ s}$ , and consequently an improvement of THD. The three-phase network voltages at the PCC and the DC bus voltage are shown in Figure 9.

The DC bus voltage regulation loop is used to keep the voltage at the terminals of the capacitor at a fixed value, in order to compensate for losses in the circuit filter and limit the variations in dynamic mode. After using the algorithm, the network voltages become balanced. The DC voltage is equivalent to about 450 V before using the filter. When the filter is switched on, the voltage is not following perfectly the reference (an error due to the unbalancing exists). Applying the fourth leg of the converter controlled by the algorithm of neutral currents neutralization, it can be observed that the voltage perfectly tracks its reference.

Fig. 10 shows the shape of the currents in the rotating frame

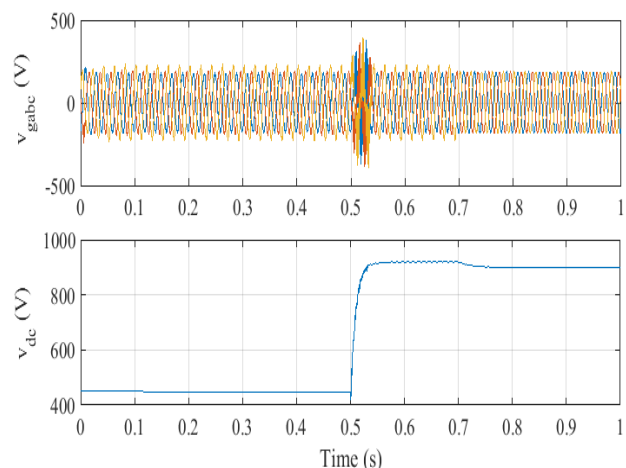


**Fig. 9** Grid PCC three-phase voltages and the filter DC bus voltage.

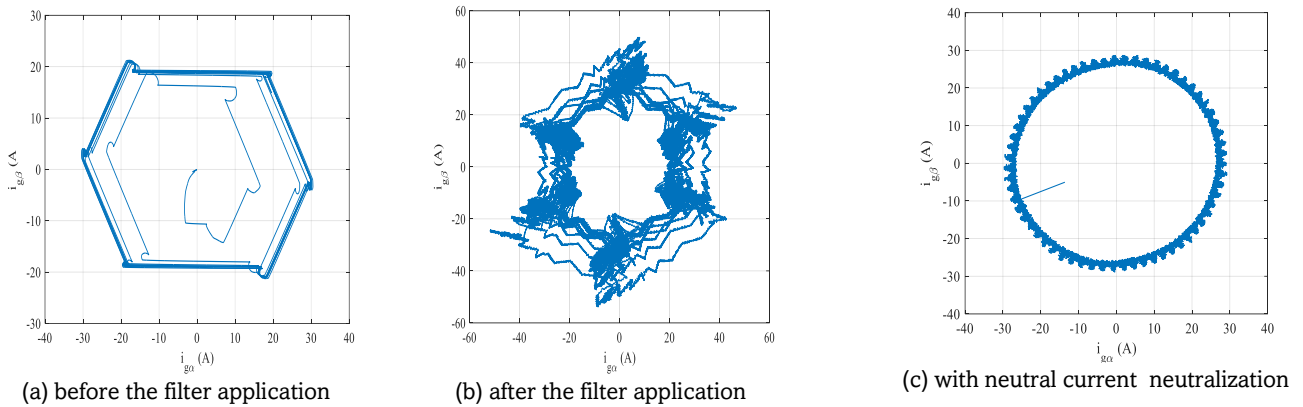


**Fig.10.** Shapes of the direct current compared to the quadratic current of the grid's reference ( $\alpha,\beta$ ).

of Concordia (direct current  $i_{g\alpha}$  and quadratic current  $i_{g\beta}$ ) for three cases (a) before the application of the filter, (b) after the application of the active filter with three arms, and (c) with the use of the fourth arm controlled by the neutral current neutralization algorithm).

It can be seen that the load unbalance directly influenced the shape of the current in the axes ( $\alpha, \beta$ ) (Fig.10a and b). The improvements made by the control system and the neutralization algorithm eliminate all unbalances of the nonlinear load and it can be noticed that the shape of the currents takes the form of a circle for case (Fig 10c) which confirms that the system becomes balanced despite the unbalance of the nonlinear load. Fig. 11 represents the spectral analysis of phase A of network voltage.

The following remarks can be drawn:

- Before filtering (Fig.11a), the distortion rate is equal to 11.98 % as measured over two periods between times 0.4 and 0.44 (sec), and the network voltage is more or less rich in harmonics.
- After filtering by three-leg inverter (Fig.11b), a slight increase in the THD is observed compared to case (a)

with a value of 12.23 %.

- After using the fourth leg (Fig.11c) the distortion rate is equal to 2.13% which shows the good filtering of the source currents.

Fig. 12 shows the FFT analysis of the current in phase A. In the literature, there are several studies in the same context (Okwako *et al.* 2022; Sundarabalan *et al.* 2019; Suresh *et al.* 2019; Chebabhi *et al.* 2015; Chebabhi *et al.* 2016). The comparative study conducted in this article is not only based on the THD of the current obtained in the various studies, but also on the complexity of the topologies and/or controls used.

In reference (Okwako *et al.* 2022), a study of a PV-battery system connected to the grid has been carried out for several scenarios. The problems of non-linear and unbalanced load were remedied by a UPQC (Unified Power Quality Conditioners). The proposed control (Artificial Neural Network) gives better results according to the recommendations of IEEE-519 standard (less than 5% THD) (Sundarabalan *et al.* 2019).

The THD obtained by the ANN control applied to the UPQC is approximately 3.3%. Similarly, a fuel cell-based system connected to the four-arm UPQC controlled by an adaptive

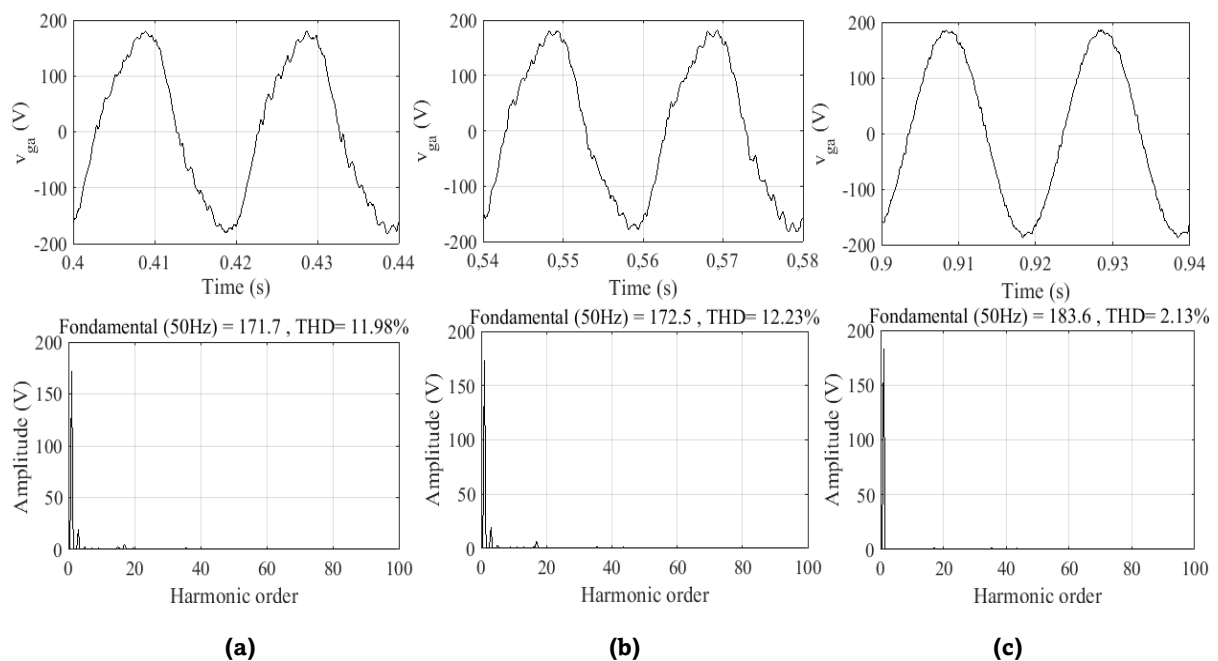


**Fig.11.** FFT voltage analysis of phase A of the network.

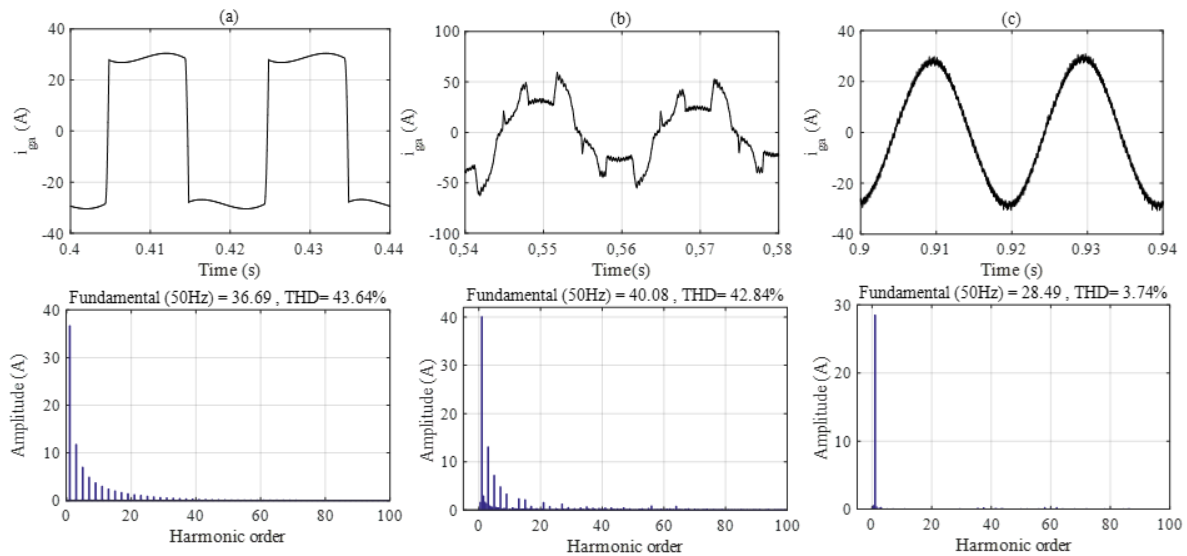


Fig.12. FFT current analysis of phase A of the network

neural regulator achieves a current THD of 2.5%. In reference (Suresh *et al.* 2019), a PV-battery and shunt active filter system are connected to a non-linear load and an imbalance in the source. The filter is controlled by fuzzy logic, and it improves the THD from 22.1% before filtering to 2.10% after filtering.

However, the complexity of either the control or topology will increase the size, weight, cost, and slower computation time for advanced controls. Our proposed approach is simple, practical, and provides an improvement in THD of 3.47% (Fig 12c) in the case of a heavily unbalanced load. A comparative study between controllers, including PI, Sliding Mode Control (MSC), and Backstepping Control, has been presented in (Chebabhi *et al.* 2015). After connecting an unbalanced and non-linear load, the comparison showed a reduction in current THD (1.68%) for the Backstepping Control compared to the other PI and MSC controls, where the THD values are 1.85% and 1.75%, respectively. The same system is also controlled by Backstepping based on 3D vector PWM, as presented in (Chebabhi *et al.* 2016). Regardless of the controls used in this article that increase the complexity of the control system, the switching frequency of the 3D vector PWM chosen is 14kHz (Chebabhi *et al.* 2015) and 10kHz (Chebabhi *et al.* 2016), which

limits the lifespan of power electronics components due to the high temperatures caused by opening and closing.

The control used allows the filter to reproduce a current in phase opposition with respect to the reference current in order to improve the THD. But the return of the current in the neutral due to the unbalance of the load (there is no information on this dismaying the command all that). In order to overcome this problem, the addition of the fourth arm is proposed with the current neutralization algorithm in the neutral as shown in Figures 8 to 12. It can be seen that our filtering system studied is not only based on the elimination of harmonics but also on compensating for the unbalance of the phases caused by the secondary load.

4.2 Reliability study of the microgrid

In this scenario, the study the behavior of the PV battery system is carried out under low solar radiation conditions (200 W/m<sup>2</sup> and 0W/m<sup>2</sup>) in order to demonstrate the efficiency of the storage system. The nonlinear load constantly consumes a power of 5kW, and the four-leg filter is activated at the beginning of the scenario.

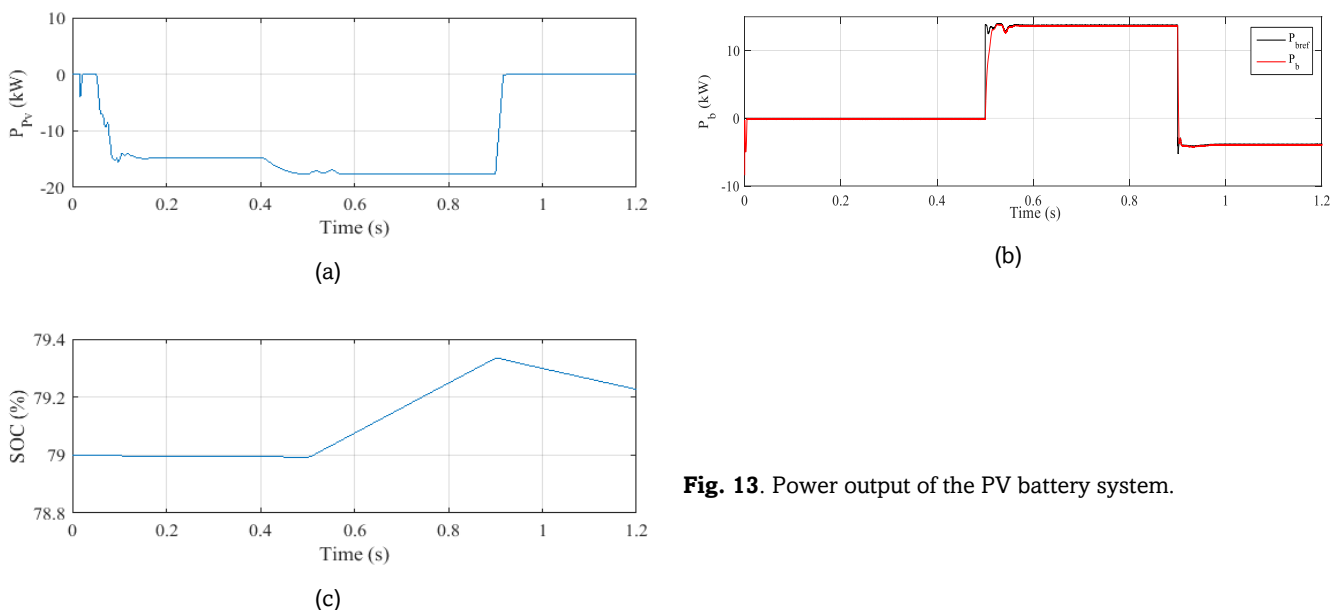


Fig. 13. Power output of the PV battery system.



Figure 13a shows the response of the power produced by the PV system. It is observed that the PV system provides (negative sign) active power to the grid in the first case ( $G=200\text{w/m}^2$ ). In the second case, the radiation becomes zero and as a result, the PV system produces no power and the power becomes zero. Figure 13b shows the power of the batteries. Initially, the storage system is idle. Once the system becomes active, the batteries consume the additional power provided by the PV system in the range [0.5, 0.9s]. In the case where the solar radiation becomes zero, the batteries produce the power required by the load (5 kW). Figure 13c shows the Battery State of Charge (SOC). It can be seen that after a fixed storage state of 79% (rest state of the storage system), the SOC increases progressively to justify the storage of the additional power by the batteries. In the remaining of this scenario, a decrease in the storage state SOC is observed due to the battery system supplying the load in the absence of PV generation. This demonstrates the effectiveness of the proposed power management system.

## 5. Conclusion

The general idea of this article is based on the influence of using a four-leg shunt active filter connected between a PV/battery system and an unbalanced non-linear load. A battery energy management algorithm controls the photovoltaic/battery hybrid system by bidirectional DC-DC converter to increase the reliability of the microgrid. This system have been simulated and evaluated using MATLAB software. The obtained results indicate the proper functioning of the filter-PV-battery system.

Moreover, based on the obtained results in which the use of the MPPT regulator proofs the increasing of the photovoltaic generator the efficiency. In the other hand, both the storage system and the energy management system have shown the availability service ensurance while considering the battery's protection by regulating the charge and discharge throughout the differents scenarios carried out. An efficiency of the control circuits against harmonics and non-linear load unbalances is shown although the current quality was improved. Hence, the THD of the current is decreased from 43.64% before filtering to the acceptable value 3.74% after filtering.

An example of simulation has been presented in order to show the advantages and the principle of operation of the four-leg PAF (parallel active filter) whose performance is often influenced by the external conditions of the electrical micro-grid (PV-batteries), the various sizing parameters as well as applied control.

According to the simulation results obtained, the instantaneous power method with the integration of the neutralization algorithm shows a good performance in the detection of reference harmonic currents. It well adapts to non-linear load variations.

## References

- Acharya, D. P., Choudhury, S., & Nayak, N. (2022). Optimal Design of Shunt Active Power Filter for Power Quality Improvement and Reactive Power Management Using nm-Predator Prey Based Firefly Algorithm. *International Journal of Renewable Energy Research (IJRER)*, 12(1), 383-397. <https://doi.org/10.20508/ijrer.v12i1.12705.g8412>
- Akagi, H., Watanabe, E. H., & Aredes, M. (2017). *Instantaneous power theory and applications to power conditioning*. John Wiley & Sons. <https://doi.org/10.1002/9780470118931.ch2>
- Albasri, F. A., Al-Mawsawi, S. A., & Al-Mahari, M. (2022). A pot line rectifier scheme with hybrid-shunt active power filter. *International Journal of Power Electronics and Drive Systems (IJPEDS)*, 13(1), 1-10. <https://doi.org/10.11591/ijpeds.v13.i1.pp1-10>
- Amini, M., Khorsandi, A., Vahidi, B., Hosseini, S. H., & Malakmahmoudi, A. (2021). Optimal sizing of battery energy storage in a microgrid considering capacity degradation and replacement year. *Electric Power Systems Research*, 195, 107170. <https://doi.org/10.1016/j.epsr.2021.107170>
- Asgharian, H., & Baniyasi, E. (2019). A review on modeling and simulation of solar energy storage systems based on phase change materials. *Journal of Energy Storage*, 21, 186-201. <https://doi.org/10.1016/j.est.2018.11.025>
- Azzam-Jai, A., & Ouassaid, M. (2019, October). Photovoltaic Interfaced Shunt Active Power Filter Under Online-Varying Parameters Based On Fuzzy Logic Controller And Adaptive Hysteresis Band Current Controller. In *2019 Third International Conference on Intelligent Computing in Data Sciences (ICDS)* (pp. 1-7). IEEE. <https://doi.org/10.1109/ICDS47004.2019.8942282>
- Barva, A. V., & Bhavsar, P. R. (2018, February). Design and simulation of four-leg based three-phase four-wire shunt active power filter. In *2018 International Conference on Communication information and Computing Technology (ICCICT)* (pp. 1-6). IEEE. <https://doi.org/10.1109/ICCICT.2018.8325868>
- Başoğlu, M. E. (2022). Comprehensive review on distributed maximum power point tracking: Submodule level and module level MPPT strategies. *Solar Energy*, 241, 85-108. <https://doi.org/10.1016/j.solener.2022.05.039>
- Belalia, K., Khodja, M., Bouzeboudja, H., Bendiabdellah, A., & Mostefa, A. (2021). Network current quality enhancement under nonlinear and unbalanced load conditions using a four-wire inverter-based active shunt filter. *Indonesian Journal of Electrical Engineering and Informatics (IJEI)*, 9(3), 601-614. <https://doi.org/10.52549/v9i3.2951>
- Benedicte, M., & Moses, P. M. (2022, August). Design of Hybrid Active Power Filters (HAPFs) for Grid-Connected Photovoltaic Systems Using Modified pq theory. In *2022 IEEE PES/IAS PowerAfrica* (pp. 1-5). IEEE. <https://doi.org/10.1109/PowerAfrica53997.2022.9905402>
- Bezerra, M. A., Oliveira, J. L., Praça, P. P., Oliveira, D. S., & Barreto, L. H. S. (2017, March). Proposal of a control scheme for an active filter on PV micro-inverter applications. In *2017 IEEE Applied Power Electronics Conference and Exposition (APEC)* (pp. 2830-2837). IEEE. <https://doi.org/10.1109/APEC.2017.7931099>
- Boukadoum, A., Bahi, T., Bouguerne, A., & Merbet, H. (2022, October). Faults Diagnosis of Active Power Filter Using Fuzzy Logic Controller under Different Conditions. In *2022 IEEE International Conference on Electrical Sciences and Technologies in Maghreb (CISTEM)* (Vol. 4, pp. 1-5). IEEE. <https://doi.org/10.1109/CISTEM55808.2022.10043886>
- Buła, D., Jarek, G., Michalak, J., & Zygmanski, M. (2021). Control method of four wire active power filter based on three-phase neutral point clamped T-type converter. *Energies*, 14(24), 8427. <https://doi.org/10.3390/en14248427>
- Challa, R. V. K., Mikkili, S., & Bonthagorla, P. K. (2022). Modeling, Controlling Approaches, Modulation Schemes, and Applications of Modular Multilevel Converter. *Journal of Control, Automation and Electrical Systems*, 1-27. <https://doi.org/10.1007/s40313-022-00953-8>
- Chebabhi, A., Fellah, M. K., Kessal, A., & Benkhoris, M. F. (2015). Comparative study of reference currents and DC bus voltage control for Three-Phase Four-Wire Four-Leg SAPF to compensate harmonics and reactive power with 3D SVM. *ISA transactions*, 57, 360-372. <https://doi.org/10.1016/j.isatra.2015.01.011>
- Chebabhi, A., Fellah, M. K., Kessal, A., & Benkhoris, M. F. (2016). A new balancing three level three dimensional space vector modulation strategy for three level neutral point clamped four leg inverter based shunt active power filter controlling by nonlinear back stepping controllers. *ISA transactions*, 63, 328-342. <https://doi.org/10.1016/j.isatra.2016.03.001>
- Chennai, S. (2022). Unified Power Quality Conditioner Performance based on Multi-level Inverter Topologies using Intelligent Controllers. *Algerian Journal of Signals and Systems*, 7(3), 109-116. <https://doi.org/10.51485/ajss.v7i3.166>

- Collins, C. T., & Green, T. C. (2022, May). DC Power Filter Design for a Neutral-Point Clamped Hybrid Multilevel Converter. *In 2022 International Power Electronics Conference (IPEC-Himeji 2022-ECCE Asia)* (pp. 2679-2686). IEEE. <https://doi.org/10.23919/IPEC-Himeji2022-ECCE53331.2022.9807067>
- de Araujo Ribeiro, R. L., Rocha, T. D. O. A., de Sousa, R. M., dos Santos, E. C., & Lima, A. M. N. (2014). A robust DC-link voltage control strategy to enhance the performance of shunt active power filters without harmonic detection schemes. *IEEE Transactions on Industrial Electronics*, 62(2), 803-813. <https://doi.org/10.1109/TIE.2014.2345329>.
- de Jesus, V. M. R., Cupertino, A. F., Xavier, L. S., Pereira, H. A., & Mendes, V. F. (2019). Comparison of MPPT strategies in three-phase photovoltaic inverters applied for harmonic compensation. *IEEE Transactions on Industry Applications*, 55(5), 5141-5152. <https://doi.org/10.1109/TIA.2019.2927924>
- Devassy, S., & Singh, B. (2017). Control of a solar photovoltaic integrated universal active power filter based on a discrete adaptive filter. *IEEE Transactions on Industrial Informatics*, 14(7), 3003-3012. <https://doi.org/10.1109/TII.2017.2778346>
- Diab, A. A. Z., Sultan, H. M., Do, T. D., Kamel, O. M., & Mossa, M. A. (2020). Coyote optimization algorithm for parameters estimation of various models of solar cells and PV modules. *IEEE Access*, 8, 111102-111140. <https://doi.org/10.1109/ACCESS.2020.3000770>
- Dobrućký, B., Kašćák, S., Šedo, J., Praženica, M., & Resutik, P. (2022). Single-Step Response and Determination of Power Components Mean Values of PES Using pq Method during Transients. *Applied Sciences*, 12(22), 11659. <https://doi.org/10.3390/app122211659>
- El Ghaly, A., Tarnini, M., Moubayed, N., & Chahine, K. (2022). A Filter-Less Time-Domain Method for Reference Signal Extraction in Shunt Active Power Filters. *Energies*, 15(15), 5568. <https://doi.org/10.3390/en15155568>
- Goud, B. S., & Rao, B. L. (2021). Power quality enhancement in grid-connected PV/wind/battery using UPQC: atom search optimization. *Journal of Electrical Engineering & Technology*, 16(2), 821-835. <https://doi.org/10.1007/s42835-020-00644-x>
- Hasan, N. S., Rosmin, N., Khalid, S., Osman, D. A. A., Ishak, B., & Mustaal, A. H. (2017). Harmonic suppression of shunt hybrid filter using LQR-PSO based. *International Journal of Electrical and Computer Engineering (IJECE)*, 7(2), 869-876. <https://doi.org/10.11591/ijece.v7i2.pp869-876>
- Hilali, A., Mardoude, Y., Ben Akka, Y., El Alami, H., & Rahali, A. (2022). Design, modeling and simulation of perturb and observe maximum power point tracking for a photovoltaic water pumping system. *International Journal of Electrical & Computer Engineering* (2088-8708), 12(4). <https://doi.org/10.11591/ijece.v12i4.pp3430-3439>
- Hoon, Y., Mohd Radzi, M. A., Hassan, M. K., & Mailah, N. F. (2016). Enhanced instantaneous power theory with average algorithm for indirect current controlled three-level inverter-based shunt active power filter under dynamic state conditions. *Mathematical Problems in Engineering*, 2016. <https://doi.org/10.1155/2016/9682512>
- Huaman, A. R. O., Monzon, I. S. O., & Diaz, E. H. V. (2022, November). Study and simulation of the use of an active filter for the mitigation of current harmonics in electrical systems. *In 2022 IEEE ANDESCON* (pp. 1-6). IEEE. <https://doi.org/10.1109/ANDESCON56260.2022.9989847>
- Kamala, S., Reddy, B. D., Sen, B., Panda, S. K., & Amaratunga, G. (2018, February). Improvement of power quality and reliability in the distribution system of petrochemical plants using active power filters. *In 2018 IEEE International Conference on Industrial Technology (ICIT)* (pp. 419-424). IEEE. <https://doi.org/10.1109/ICIT.2018.8352214>
- Khalid, S., & Kumar, S. (2020). ANFIS-SCC Control of Shunt Active Power Filter for Minimization of Harmonics for More Electric Aircraft System. *In Applications of Artificial Intelligence in Electrical Engineering* (pp. 1-22). IGI Global. <https://doi.org/10.4018/978-1-7998-2718-4.ch001>
- Kumar, M., Uqaili, M. A., Memon, Z. A., & Das, B. (2022). Experimental Harmonics Analysis of UPS (Uninterrupted Power Supply) System and Mitigation Using Single-Phase Half-Bridge HAPF (Hybrid Active Power Filter) Based on Novel Fuzzy Logic Current Controller (FLCC) for Reference Current Extraction (RCE). *Advances in Fuzzy Systems*, 2022. <https://doi.org/10.1155/2022/5466268>
- Kumar, T. S., & Shanmugam, J. (2020). Application of ANFIS Controller to 3-Level NPC Based APF to Improve Power Quality. *Journal of Critical Reviews*, 7(14). <https://doi.org/10.31838/jcr.07.14.57>
- Maciel, L. F. A., Morales, J. L. M., Gaona, D. C., & Pimentel, J. G. M. (2018, November). A study of a three-phase four-wire shunt active power filter for harmonics mitigation. *In 2018 IEEE International Autumn Meeting on Power, Electronics and Computing (ROPEC)* (pp. 1-6). IEEE. <https://doi.org/10.1109/ROPEC.2018.8661416>
- Mankour, S. E., Belarbi, A. W., & Benmessaoud, M. T. (2017). Modeling and Simulation of a Photovoltaic Field for 13 KW. *International Journal of Electrical & Computer Engineering* (2088-8708), 7(6). <https://doi.org/10.11591/ijece.v7i6.pp3271-3281>
- Nayak, B. P., & Shaw, A. (2017, January). Design of MPPT controllers and PV cells using MATLAB Simulink and their analysis. *In 2017 International Conference on Nascent Technologies in Engineering (ICNTE)* (pp. 1-6). IEEE. <https://doi.org/10.1109/ICNTE.2017.7947932>
- Okay, K., Eray, S., & Eray, A. (2022). Development of prototype battery management system for PV system. *Renewable Energy*, 181, 1294-1304. <https://doi.org/10.1016/j.renene.2021.09.118>
- Okwako, O. E., Lin, Z. H., Xin, M., Premkumar, K., & Rodgers, A. J. (2022). Neural Network Controlled Solar PV Battery Powered Unified Power Quality Conditioner for Grid Connected Operation. *Energies*, 15(18), 6825. <https://doi.org/10.3390/en15186825>
- Olabi, A. G., Wilberforce, T., Sayed, E. T., Abo-Khalil, A. G., Maghrabie, H. M., Elsaid, K., & Abdelkareem, M. A. (2022). Battery energy storage systems and SWOT (strengths, weakness, opportunities, and threats) analysis of batteries in power transmission. *Energy*, 254, 123987. <https://doi.org/10.1016/j.energy.2022.123987>
- Patel, A., Joshi, S., & Mehta, B. (2020). Comparative analysis for INC and P&O MPPT based photovoltaic energy conversion system. *In Advances in Control Systems and its Infrastructure* (pp. 147-159). Springer, Singapore. [https://doi.org/10.1007/978-981-15-0226-2\\_12](https://doi.org/10.1007/978-981-15-0226-2_12)
- Pradhan, A., & Panda, B. (2017). Experimental analysis of factors affecting the power output of the PV module. *International Journal of Electrical and Computer Engineering*, 7(6), 3190. <https://doi.org/10.11591/ijece.v7i6.pp3190-3197>
- Raman, R., Sadhu, P. K., Kumar, R., Rangarajan, S. S., Subramaniam, U., Collins, E. R., & Senjyu, T. (2022). Feasible Evaluation and Implementation of Shunt Active Filter for Harmonic Mitigation in Induction Heating System. *Electronics*, 11(21), 3464. <https://doi.org/10.3390/electronics11213464>
- Rao, K. K., Rao, P. B. K., & Abishai, T. (2017). Power quality enhancement in grid connected PV systems using high step up DC-DC converter. *International Journal of Electrical and Computer Engineering*, 7(2), 720. <https://doi.org/10.11591/ijece.v7i2.pp720-728>
- Rasul, M. J., Khang, H. V., & Kolhe, M. (2017, August). Harmonic mitigation of a grid-connected photovoltaic system using shunt active filter. *In 2017 20th International Conference on Electrical Machines and Systems (ICEMS)* (pp.1-5) IEEE. <https://doi.org/10.1109/ICEMS.2017.8056401>
- Rath, A., & Srungavarapu, G. (2022). An Advanced Shunt Active Power Filter (SAPF) for Non-ideal Grid Using Predictive DPC. *IETE Technical Review*, 1-14. <https://doi.org/10.1080/02564602.2022.2127946>
- Rohouma, W., Balog, R. S., Peerzada, A. A., & Begovic, M. M. (2020). D-STATCOM for harmonic mitigation in low voltage distribution network with high penetration of nonlinear loads. *Renewable Energy*, 145, 1449-1464. <https://doi.org/10.1016/j.renene.2019.05.134>
- Saleh, K., & Madi, A. (2021). A fault-tolerant photovoltaic integrated shunt active power filter with a 27-level inverter. *International Journal of Electrical and Computer Engineering (IJECE)*, 11(2), 1166-1177. <https://doi.org/10.11591/ijece.v11i2.pp1166-1177>
- Sundarabalan, C. K., Puttagunta, Y., & Vignesh, V. (2019). Fuel cell integrated unified power quality conditioner for voltage and current reparation in four-wire distribution grid. *IET Smart Grid*, 2(1), 60-68. <https://doi.org/10.1049/iet-stg.2018.0148>
- Suresh, P., & Vijayakumar, G. (2020). Shunt active power filter with solar photovoltaic system for long-term harmonic mitigation. *Journal of Circuits, Systems and Computers*, 29(05), 2050081. <https://doi.org/10.1142/S02181266200500814>
- Tounsi, M. M., Allali, A., Merabet Boulouiha, H., & Denai, M. (2021). ANFIS control of a shunt active filter based with a five-level NPC inverter to improve power quality. *International Journal of Electrical and Computer Engineering*. <https://doi.org/10.11591/ijece.v11i3.pp1886-1893>

- Tsvetanov, D., Djagarov, N., Grozdev, Z., & Djagarova, J. (2022, June). Harmonic Compensation in Ship Power System Using pq Theory Control Based Shunt Active Power Filter. In *2022 8th International Conference on Energy Efficiency and Agricultural Engineering (EE&AE)* (pp. 1-10). IEEE. <https://doi.org/10.1109/EEAE53789.2022.9831307>
- Wu, D., Ma, X., Fu, T., Hou, Z., Rehm, P. J., & Lu, N. (2022). Design of a Battery Energy Management System for Capacity Charge Reduction. *IEEE Open Access Journal of Power and Energy*, 9, 351-360. <https://doi.org/10.1109/OAJPE.2022.3196690>
- Zhang, B., Ping, S., Long, Y., Jiao, Y., & Wu, B. (2022). Research on topology of a novel three-phase four-leg fault-tolerant NPC inverter. *Archives of Electrical Engineering*, 71(2). <https://doi.org/10.24425/aee.2022.140724>
- Zhang, L., Li, X., Yang, M., & Chen, W. (2021). High-safety separators for lithium-ion batteries and sodium-ion batteries: advances and perspective. *Energy Storage Materials*, 41, 522-545. <https://doi.org/10.1016/j.ensm.2021.06.033>



© 2023. The Author(s). This article is an open access article distributed under the terms and conditions of the Creative Commons Attribution-ShareAlike 4.0 (CC BY-SA) International License (<http://creativecommons.org/licenses/by-sa/4.0/>)